18th International Conference on Space Operations, Montreal, Canada, 26 - 30 May 2025.

SpaceOps-2025, ID # 238

SCISAT Extending a two-year Mission into Decades of Scientific Discoveries – An Attitude-Independent Magnetometer Calibration in non-uniform Magnetic Field

Justin St-Charles ing.[a]

[a] *Calian Advanced Technologies, Canadian Space Agency, 6767 route de l'Aéroport, Saint-Hubert, Québec, J3Y 8Y9, Canada.* *justin.st-charles@calian.com*

Abstract

SCISAT is a slow-spinning Spacecraft with an approximate four-month beta cycle, occultation science being at the very heart of its activities. With a nominal mission life of 2 years, the Spacecraft launched in 2003 still proves invaluable today in obtaining relevant scientific data. After losing its sole star tracker in June 2015, SCISAT was left without the capability to have its onboard Magnetometer further calibrated (offline process). After almost a decade without calibration, it was feared that some attitude disturbances experienced in early 2023 could be rooted in the Magnetometer's degraded performance, since that equipment is the only remaining attitude determination sensor nominally available in eclipse, when the Fine Sun Sensor is useless.

In an effort to improve the situation, the implementation of an Attitude-Independent algorithm, based on some papers released roughly between 2005 and 2015, was studied. The adaptation for non-uniform magnetic field was derived and existing telemetry was processed offline. Although the alignment of the equipment remains an outstanding difficulty, the updated calibration method was successful in reproducing similar performance to the previous years of calibration campaigns within an acceptable degree of precision, in view of the mission requirements. Comparison of several such campaigns for times where star tracker data was available as a reference allows to isolate a mean alignment orientation which, as long as proven stable in time to an adequate degree of precision, can successfully be used to process contemporary data.

The calibration parameters estimated using the 2024 data were implemented for a flight test, whereby the impacts on attitude determination performance have begun being collected for analysis. Although at time of writing, slightly less than half a beta cycle of data is available, early results already exhibit a trend of decreased attitude errors compared to the previous year.

Keywords: SCISAT, Magnetometer, Calibration, Attitude-Independent, Varying B-Field

Nomenclature

$\mathbf{b}$	Calibration bias vector $\in \mathbb{R}^3$, in the sensor frame
$\mathbf{d}$	Calibration bias vector (compound) $\in \mathbb{R}^3$, in the body frame
$\mathbf{h}_{ri}$	Magnetometer raw measurement $\in \mathbb{R}^3$, for a given telemetry point
H_{REFi}	Reference magnetic field magnitude $\in \mathbb{R}$, for a given telemetry point
$\mathbf{h}_{REFi}$	Reference magnetic field vector $\in \mathbb{R}^3$, in body frame, for a given telemetry point
$\mathbf{h}_{POLY}$	Biased reference magnetic field vector $\in \mathbb{R}^3$, in body frame, for a given telemetry point
λ’	Signed non-orthogonality angle between Y-sensor and the corresponding Y orthogonal axis
$\mathbf{P}$	Calibration adjustment matrix $\in GL(3, \mathbb{R})$, in the body frame
φ’	Signed non-orthogonality angle between Z-sensor and the XZ orthogonal plane
$\mathbf{R}$	Alignment rotation Matrix $\in SO(3, \mathbb{R})$ (from sensor frame to body frame)
ρ’	Signed non-orthogonality angle between Z-sensor and the YZ orthogonal plane
$\mathbf{T}$	Calibration adjustment matrix $\in GL(3, \mathbb{R})$, in the sensor frame
σ^2_{mi}	Variance

Acronyms/Abbreviations

ADCS	Attitude Determination and Control System
B	Magnetic (Field)
CSA	Canadian Space Agency
DoY	Day of Year
FSW	Flight Software
FTS	Fourier Transform Spectrometer
IGRF	International Geomagnetic Reference Field
MAESTRO	Measurements of Aerosol Extinction in the Stratosphere and Troposphere Retrieved by Occultation
MLE	Maximum likelihood Estimation
RMS	Root Mean Square
RSS	Root Sum Squared
WLSM	Weighted Least Squares Method

1. Introduction

Ever since it was launched in August 2003, SCISAT performs daily science readings as part of CSA space science program using notably its Fourier Transform Spectrometer (FTS) and MAESTRO instruments, to provide a worldwide team of researchers with valuable data on the chemistry at play in the stratosphere regarding mainly the depletion of the ozone layer and has led to many discoveries in that field over the years, as well as the detection of many pollutants injected in the atmosphere.

Initially designed to fulfil the needs of a two-year mission, the ADCS equipment of SCISAT features little to no redundancy, and the sole star tracker was lost to a fault back in June 2015. The remaining sensors onboard in nominal use are the coarse and fine sun sensors, as well as the magnetometer. The FSS keeps the alignment of the sun vector along the body X axis at all times whenever the sun is present (determining Pitch and Yaw errors), leaving the magnetometer, a Billingsley TFM100S, in charge of solving for the remaining Roll angle. Due to the nature of its mission requirements, the Spacecraft has a revolving beta cycle and experiences an eclipse each orbit for most of its four-month beta cycle. During eclipse, only the Roll angle is actively controlled by the FSW using the magnetometer measurements, while the Pitch and Yaw are temporarily left in open loop.

The pointing budget for SCISAT is not particularly stringent. As pointed out in [4], the optimal parameters of the magnetometer calibration are time-varying on-orbit, but also during the beta cycle as a whole. Since the elected calibration scheme for SCISAT operations involves the use of constant parameters, the yearly calibration strives to establish the mean optimal parameters only. Consequently, even up to 2014 when the calibration was conducted offline routinely using typical attitude-dependent WLSM optimization [5] using the star tracker telemetry, the perceived attitude errors are seen to make rather sizable jumps during eclipse when the magnetometer is the only means of attitude determination. For the Pitch and Yaw angles in particular, not subject to closed-loop control in absence of the sun, attitude errors exhibit frequent degradations around 0.02 rad in order of magnitude.

The loss of the star tracker marked the end of the yearly magnetometer calibration process, since the instrument readings were a necessary input for the algorithm. For over a decade, the same parameters were consequently maintained in the FSW. From the few last calibration campaigns, the parameter values were known to have stabilized to a great extent, the last two analyses having actually recommended no operational update to the 2012 adjustment, on account of the very small observed evolution not meeting the primary criterion of the average deviation to the B-field vector plus 3-sigma being above 0.5 mG. However, following a momentary perceived loss of fine attitude (limit of 0.1 rad magnitude) in early 2023 at occultation transitions, causing a mode transition needing a manual recovery – depicted in Fig. 1 – as well as a 2024 near-miss around the same date, it was conjectured that a re-calibration, if achieved, could help reduce the coupling of attitude errors and decrease the odds of possible re-occurrence of such ADCS difficulties. A survey of the possibilities to re-establish a means of calibration was therefore conducted.

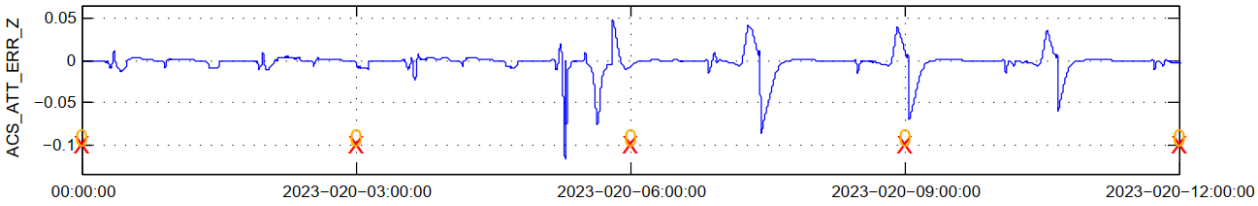

Fig. 1. Loss of fine attitude in January 2023

Although the Spacecraft documentation [6] provided for the possible unavailability of the star tracker by relying on the FSS to produce the necessary attitude determination, the corresponding array of solutions possessed the known shortcomings of needing to deter the Spacecraft from its nominal pointing for several days to create a 10 to 20 degree angle between the instrument axis and the sun vector, as well as truncating the available telemetry dataset to about half, which in turn would lead to unquantified uncertainties with respect to the achievable performance, due to the time-varying nature of the optimal calibration. The focus of the study was hence cast on the Attitude-Independent schemes, for which an abundant literature now exists, that features many variations. In searching constant parameters through offline processing of rather large amounts of telemetry, the MLE formulation proposed in [1] and commented in [2] was elected for the study, which itself builds on several variations related to the so-called Twostep formulation

[3, 7, 8]; the interested reader may be directed to a review of the cited papers for a thorough account of literature. The method, developed for time-invariant parameters and a constant reference magnetic field, had to be extended to non-uniform B-field and as will be seen, could yield good results for on-orbit datasets.

A succinct account of the followed methodology is presented in Section 2, focusing on the actual variations from [1, 2], and the results of the preliminary conducted tests, the prospects of the possible alignment method, and early results of the flight implementation are then provided in Section 3.

2. Methodology

As previously stated, the studied calibration scheme closely follows [1, 2] and proceeds conceptually as outlined in Figure 2, in which the darker blocks can be realized only when an external reference attitude determination is possible – in the case of SCISAT, up to the year 2014:

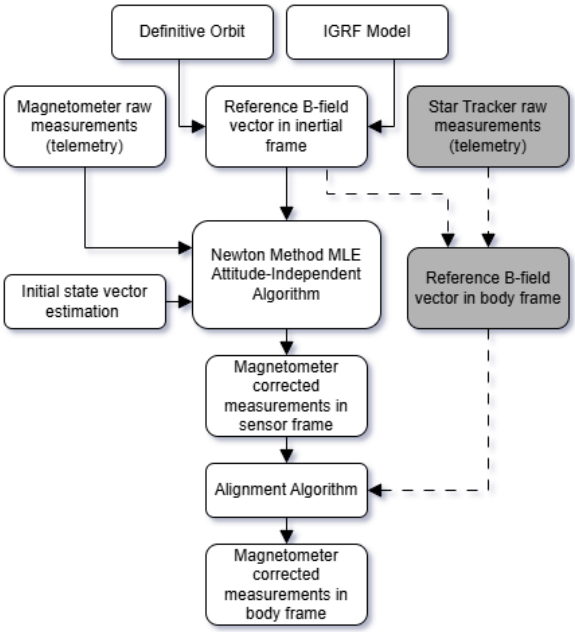

Fig. 2. Methodology Flowchart

The analysis depends on the following:

A) The telemetry for the onboard magnetometer raw measurements. For SCISAT, it is provided in pseudo-body frame, as the sensor frame readings are passed to body frame by axes re-identification (the quality of the calibration demonstrated that an additional small-angle alignment is in fact necessary). Following the treatment of the former calibration process to alleviate the analysis of comparative metrics, typically between 700,000 and 1,100,000 telemetry points sampled at 1 Hz for this data had to be parsed for each year, pertaining to 9 days chosen to represent 9 specific beta angles, over half a beta cycle. The selected beta angles are {0°, ±10°, ±20°, ±40°, ±60°}; higher beta angles are not represented, since science typically is not taken above this range, when the Spacecraft experiences no eclipses.

B) The reference B-field available in inertial frame, as calculated on the ground. The precision of this data depends on the standing IGRF model as well as the ground-calculated definitive orbit determination. For SCISAT, this data is available every 2 seconds and was linearly interpolated as needed to complement each magnetometer telemetry point.

C) The telemetry from the star tracker, whenever available (for datasets up to 2014), used as the attitude reference frame to convert the reference B-field to the assumed actual body frame. For SCISAT, the star tracker precision is nominally estimated at 0.0792° [9], but is disregarded in the present processing, as its reference frame is considered absolute. That historical data is also available at 1 Hz frequency and was also linearly interpolated as needed to augment the magnetometer readings timestamps.

A full account of the error sources at play, which are manifold, is left out of scope for the needs of the present paper. Besides the ignored star tracker precision and the mean alignment impacts that will be discussed below, precision is further dependent on the precision of the IGRF model itself (given at 10 nT RMS plus the secular variation of 20 nT/year [10]), that of the definitive orbit determination, the magnetometer digitization error of 31.73 nT [9], etc.

2.1 Initial Parameters Estimation

The first step of the calibration process consists of achieving an initial estimate of the parameters as a starting point to ensure convergence on a valid set of solutions during the second step.

In the literature [1, 3], a means of establishing the estimation via parametric ellipsoid fitting (least squares estimator) is provided, but the development is available only in the simpler case where the magnetic field is constant. It is not clear on the outset whether a variation on the method may be harnessed for the initial estimation step in case of a non-constant B-field, as is the case on-orbit. While an extension of the fitting to the non-uniform case was tried and yielded promising results on small gaussian-noised simulated datasets, the method is not yet mature for presentation when applied to large datasets of on-orbit telemetry. However, since the attempted method relied on a system of solutions mostly collapsing to that of [1], some side notes in its respect can be added in hope to prove beneficial:

1) Alternate derivations to obtain the values of φ and β_2 can be proposed – all variables following the nomenclature of [1], Appendix A:

$$\sin(\varphi) = \frac{(BE-2CD)}{\sqrt{-\alpha_3}} \tag{1}$$

$$\beta_2 = -2\mathrm{AEI} - 4\mathrm{AH} + \mathrm{BCI} + 2\mathrm{BG} - \mathrm{C}^2\mathrm{H} + \mathrm{CEG} \tag{2}$$

2) The sign ambiguity on the several roots can be lifted in the case of the variables a, b and c by using the fact that those scaling factors remain close to unity in practice and hence will assume positive final values. It appears that the sign ambiguity in the case of the non-orthogonality angles ρ, φ and λ can be lifted by ensuring that the development for each coefficient of the ellipse equation [1, 3] holds; namely, for instance, denoting by ρ', φ' and λ' the correctly signed angles, their final values can be inferred using the following formulae in sequence, assuming small angles:

$$\lambda' = \mathrm{asin}\left(\frac{E*cos(\rho)*b}{2c}\right) \tag{3}$$

$$\varphi' = \mathrm{asin}\left(\frac{B*a*b*cos^2(\rho)+c*C*a*\left(sin^2(\lambda\prime)+cos^2(\lambda)*cos^2(\varphi)\right)*\frac{cos(\rho)}{sin(\lambda\prime)}}{2c^2\left[\left(sin^2(\lambda\prime)+cos^2(\lambda)*cos^2(\varphi)\right)*\frac{cos(\rho)}{tan(\lambda\prime)}-sin(\lambda\prime)*cos(\rho)*cos(\lambda)\right]}\right) \tag{4}$$

$$\rho' = \mathrm{asin}\left(\frac{2c*sin(\varphi\prime)*cos(\lambda)*cos(\rho)-C*a*cos(\rho)}{2c*sin(\lambda\prime)}\right) \tag{5}$$

In the case of SCISAT however, the historical calibration parameters were already available. In the present state of the analysis, an initial state vector was established that was used uniformly in all the runs, in an attempt to promote consistency during the alignment phase.

2.2 Maximum Likelihood Estimator

The core of the algorithm is to implement a Newton method using explicit formulation for the Gradient and Hessian. Since the relevant literature [1, 2] is found to cover essentially the case of uniform (constant) reference B-field, the results were re-derived for the non-constant case. To the author's knowledge, this simple adaptation was not made available, although hinted at in [1]. The derivation is provided both for the optimization problem presented in [1], and that used as a basis in [2], the latter of which was retained to produce final results in the present analysis, albeit with seemingly little practical difference.

For the optimization problem (as stated in [1])

$$\min \sum_{i=1}^{n} \left(\frac{\|\mathbf{T}(\mathbf{h}_{ri}-\mathbf{b})\|-1}{\sigma_{mi}} \right)^2 \tag{6}$$

leading to the modified problem

$$\min \sum_{i=1}^{n} \left(\frac{\|\mathbf{T}(\mathbf{h}_{ri}-\mathbf{b})\|-\|\mathrm{H}_{REFi}\|}{\sigma_{mi}} \right)^2 \tag{7}$$

the formulation for the Gradient and Hessian sub-matrices in non-uniform magnetic field becomes – all variables following the nomenclature of [1], Appendix B:

$$\nabla f|_{\mathbf{T}} = \sum_{i=1}^{n} \frac{2\left(1-\frac{\|\mathrm{H}_{REFi}\|}{\|\mathbf{T}\mathbf{u}_i\|}\right)}{\sigma_{mi}^2} \, \mathbf{u}_i \otimes \mathbf{T}\mathbf{u}_i \tag{8}$$

$$\nabla f|_{\mathbf{b}} = \sum_{i=1}^{n} \frac{-2\left(1-\frac{\|\mathrm{H}_{REFi}\|}{\|\mathbf{T}\mathbf{u}_i\|}\right)}{\sigma_{mi}^2} \, \mathbf{T}^T\mathbf{T}\mathbf{u}_i \tag{9}$$

$$\mathbf{H}_{\mathbf{T},\mathbf{T}} = \sum_{i=1}^{n} \frac{2}{\sigma_{mi}^2} \left[\frac{(\mathbf{u}_i\mathbf{u}_i^T)\otimes(\mathbf{T}\mathbf{u}_i\mathbf{u}_i^T\mathbf{T}^T)}{\|\mathbf{T}\mathbf{u}_i\|^3} \|\mathrm{H}_{REFi}\| + \left(1-\frac{\|\mathrm{H}_{REFi}\|}{\|\mathbf{T}\mathbf{u}_i\|}\right)[(\mathbf{u}_i\mathbf{u}_i^T)\otimes\mathbf{I}_3] \right] \tag{10}$$

$$\mathbf{H}_{\mathbf{T},\mathbf{b}} = \sum_{i=1}^{n} \frac{-2}{\sigma_{mi}^2} \left[\frac{(\mathbf{u}_i\otimes\mathbf{T}\mathbf{u}_i)\mathbf{u}_i^T\mathbf{T}^T\mathbf{T}}{\|\mathbf{T}\mathbf{u}_i\|^3} \|\mathrm{H}_{REFi}\| + \left(1-\frac{\|\mathrm{H}_{REFi}\|}{\|\mathbf{T}\mathbf{u}_i\|}\right)(\mathbf{u}_i\otimes\mathbf{T} + \mathbf{I}_3\otimes\mathbf{T}\mathbf{u}_i) \right] \tag{11}$$

$$\mathbf{H}_{\mathbf{b},\mathbf{b}} = \sum_{i=1}^{n} \frac{2}{\sigma_{mi}^2} \left[\frac{\mathbf{T}^T\mathbf{T}\mathbf{u}_i\mathbf{u}_i^T\mathbf{T}^T\mathbf{T}}{\|\mathbf{T}\mathbf{u}_i\|^3} \|\mathrm{H}_{REFi}\| + \left(1-\frac{\|\mathrm{H}_{REFi}\|}{\|\mathbf{T}\mathbf{u}_i\|}\right)\mathbf{T}^T\mathbf{T} \right] \tag{12}$$

Whereas for the equivalent optimization problem aligned with [2]

$$\min \sum_{i=1}^{n} \left(\frac{1-\|\mathbf{T}(\mathbf{h}_{ri}-\mathbf{b})\|^2}{\sigma_{mi}} \right)^2 \tag{13}$$

The formulation for the Gradient and Hessian sub-matrices in non-uniform magnetic field yielded – all variables following the nomenclature of [1], Appendix B:

$$\nabla f|_{\mathbf{T}} = \sum_{i=1}^{n} \frac{4\left(\|\mathbf{T}\mathbf{u}_i\|^2-\|\mathrm{H}_{REFi}\|^2\right)}{\sigma_{mi}^2\|\mathrm{H}_{REFi}\|^2} \, \mathbf{u}_i \otimes \mathbf{T}\mathbf{u}_i \tag{14}$$

$$\nabla f|_{\mathbf{b}} = \sum_{i=1}^{n} \frac{-4\left(\|\mathbf{T}\mathbf{u}_i\|^2-\|\mathrm{H}_{REFi}\|^2\right)}{\sigma_{mi}^2\|\mathrm{H}_{REFi}\|^2} \, \mathbf{T}^T\mathbf{T}\mathbf{u}_i \tag{15}$$

$$\mathbf{H_{T,T}} = \sum_{i=1}^{n} \frac{4}{\sigma_{mi}^2 \|\mathrm{H}_{REFi}\|^2} \left[2(\mathbf{u}_i\mathbf{u}_i^T)\otimes(\mathbf{T}\mathbf{u}_i\mathbf{u}_i^T\mathbf{T}^T) + (\|\mathbf{T}\mathbf{u}_i\|^2 - \|\mathrm{H}_{REFi}\|^2)[(\mathbf{u}_i\mathbf{u}_i^T)\otimes\mathbf{I}_3]\right] \quad (16)$$

$$\mathbf{H_{T,b}} = \sum_{i=1}^{n} \frac{-4}{\sigma_{mi}^2 \|\mathrm{H}_{REFi}\|^2} \left[2(\mathbf{u}_i\otimes\mathbf{T}\mathbf{u}_i)\mathbf{u}_i^T\mathbf{T}^T\mathbf{T} + (\|\mathbf{T}\mathbf{u}_i\|^2 - \|\mathrm{H}_{REFi}\|^2)(\mathbf{u}_i\otimes\mathbf{T} + \mathbf{I}_3\otimes\mathbf{T}\mathbf{u}_i)\right] \quad (17)$$

$$\mathbf{H_{b,b}} = \sum_{i=1}^{n} \frac{4}{\sigma_{mi}^2 \|\mathrm{H}_{REFi}\|^2} \left[2\mathbf{T}^T\mathbf{T}\mathbf{u}_i\mathbf{u}_i^T\mathbf{T}^T\mathbf{T} + (\|\mathbf{T}\mathbf{u}_i\|^2 - \|\mathrm{H}_{REFi}\|^2)\mathbf{T}^T\mathbf{T}\right] \quad (18)$$

It should be noted that in the current state of the conducted analysis for SCISAT, the variance term σ_{mi} was replaced by unit weight in all computations for simplicity, following [2], under assumption that the curvature effect mentioned in [1] be negligible, in view of the close to spherical fit observed in previous calibration campaigns.

2.2 Final Alignment

As highlighted in [1], alignment remains an outstanding issue after completion of the main steps of the algorithm. Because the calibration parameters are found in the sensor frame, failure to correct any small difference to the actual body frame translates to direct attitude misestimation. For the SCISAT datasets where the star tracker telemetry was available, solving for the optimal alignment was possible by following [1].

In practice, the calibration parameters for SCISAT are broken down in two distinct sets: the linear biases are not processed onboard but are deduced from each reference B-field vector the Spacecraft is provided with, which must be in true body frame. On the contrary, the matrix of scaling parameters – the T-Matrix, following the naming convention in [1] – is uplinked to the Spacecraft to be used by the FSW in processing the raw measurements. Accounting for the T-matrix to be a rank two tensor fully passed from a frame 1 to a frame 2 by the general formula

$$\mathbf{T_2} = \mathbf{R}\mathbf{T_1}\mathbf{R}^T \quad (19)$$

the uplinked scaling parameters matrix **P** and true body frame bias vector **d** used by the ground for the SCISAT operations are established from the algorithm output T-matrix and bias vector **b** (both found in sensor frame, or the unaligned pseudo-body frame) through left-multiplication only by the pseudo-body frame to true body frame alignment matrix R, like so:

$$\mathbf{RT}(\mathbf{h}_{ri} - \mathbf{b}) \approx \mathbf{h}_{REFi} \quad (20)$$

$$\mathbf{RT}\mathbf{h}_{ri} \approx \mathbf{h}_{REFi} + \mathbf{RT}\mathbf{b} \quad (21)$$

Identifying **P** = **RT** and **d** = **RTb**:

$$\mathbf{P}\mathbf{h}_{ri} \approx \mathbf{h}_{REFi} + \mathbf{d} = \mathbf{h}_{POLY} \quad (21)$$

With $\mathbf{h}_{POLY}$ the biased B-field vector in true body frame provided by the ground to the Spacecraft as a polynomial, and **P** being further converted by axes re-identification.

3. Results and discussion

The analysis was first conducted on the data pertaining to six reference years – from 2009 to 2014 – for which both the star tracker telemetry and the results of the previous yearly calibration routine were readily available, so as to assess performance. This also ensured that the final optimal alignment process could be achieved and allowed investigation with respect to the possible subsequent use of a mean alignment. The analysis was then performed on the datasets of 2023 and 2024, and the resulting calibration parameters were implemented for a flight test.

3.1 Mean Alignment Determination

Following the analysis on each year of the reference interval, the alignment of the adjusted magnetometer measurements in the sensor frame was done by solving the corresponding Wahba's problem, using the star tracker to provide the body frame reference.

Table 1. Roll-Pitch-Yaw alignment angles for the years 2009-2014

	Average [°]	**2009**	**2010**	**2011**	**2012**	**2013**	**2014**
Roll	0.291	+0.086	-0.007	-0.026	-0.031	-0.042	+0.020
Pitch	-0.491	-0.002	+0.004	+0.003	+0.011	-0.020	+0.003
Yaw	-0.440	-0.001	-0.007	+0.016	+0.010	-0.020	+0.002

In view of SCISAT's pointing budget, the scatters of the extracted alignments Roll, Pitch and Yaw, depicted in Table 1, were found to be relatively small, which served as a basis to the hypothesis that a mean alignment could prove adequate to apply the new algorithm in absence of reference attitude telemetry. It was conjectured that albeit a residual rotational error in SO(3, $\mathbb{R}$) would remain, and despite the fact that the calibration consequently would not be found optimal in the general case, the residual error could prove sufficiently small to still allow for an improvement compared to the standing calibration parameters of SCISAT.

It is noteworthy that the actual optimal alignment was demonstrated to also vary during the orbit, at least for the selected starting state vector. As exemplified by Fig. 3, conducted tests featuring colatitude cutoff values truncating the datasets by means of an extra parametric value exhibit smooth curves in the resulting isolated Roll-Pitch-Yaw alignment angles output; in the case of Roll, sweeping about a full degree. Testing suggests these curves may be flattened, as influenced by the starting initial state vector estimate but, as will be discussed below, better overall performance could not be achieved.

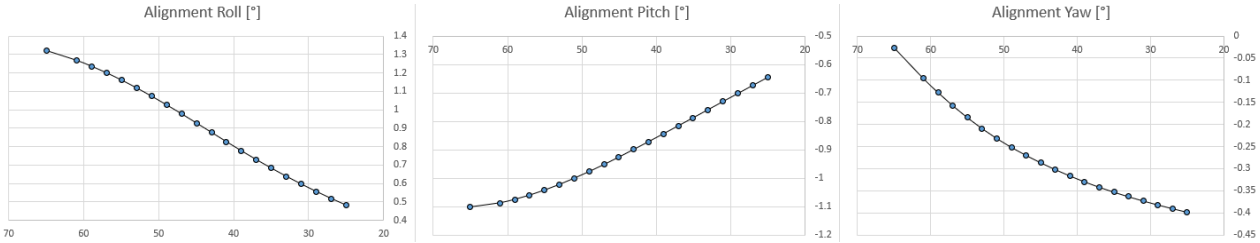

Fig. 3. Optimal alignment angles for 20 runs sweeping 65° to 25° Colatitude cutoff, 2014 dataset

3.2 Comparative Results on the reference datasets (2009-2014)

The results for each year of the reference interval were computed with the replacement algorithm both after optimal alignment and after mean alignment using the mean alignment described above. Fig. 4 shows a one-day example of the comparative adjusted curves for the former WLSM methodology, MLE new algorithm with optimal alignment (the attitude reference being provided by the star tracker) and MLE new algorithm with mean alignment (no attitude knowledge), showcasing that the resulting impact on the performance, although quantitively noticeable, still remains of relatively small magnitude.

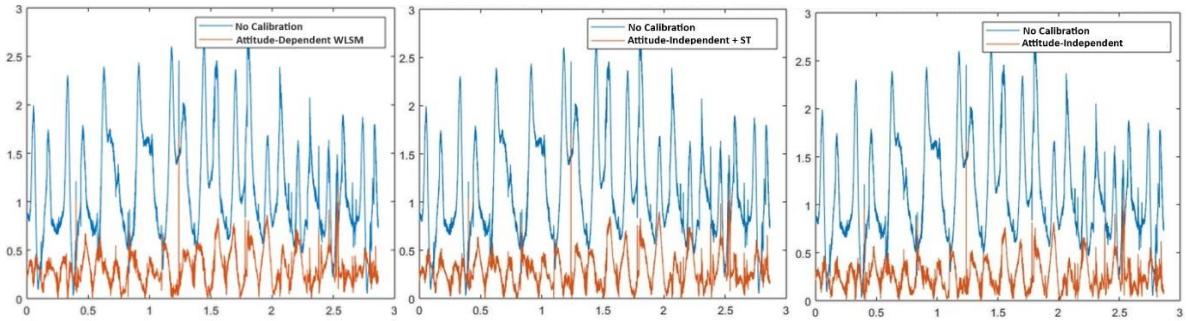

Fig. 4. Angle [°] between the magnetometer measurement and the B-field vector for three calibration methods, typical day of the 2009 dataset (Oct. 24th)

Table 2. Calibration Performance Comparative Metrics, Measured B-Field vs Reference B-Field Vectors, 2009

2009			**Former WLSM**	**New MLE, Optimal Alignment**	**New MLE, Mean Alignment**
X axis	**Avg.**	**[mG]**	0.20	0.09	0.09
	Std. Dev.	**[mG]**	1.79	1.53	1.53
	Avg.+3σ	**[mG]**	5.58	4.74	4.74
Y Axis	**Avg.**	**[mG]**	0.01	-0.21	-0.24
	Std. Dev.	**[mG]**	1.43	1.33	1.38
	Avg.+3σ	**[mG]**	4.38	4.21	4.39
Z Axis	**Avg.**	**[mG]**	0.08	0.20	0.22
	Std. Dev.	**[mG]**	1.73	1.62	1.60
	Avg.+3σ	**[mG]**	5.28	5.06	5.00
RSS	**Avg.+3σ**	**[mG]**	8.87	8.16	8.21
Final Angle	**Avg.**	[°]	0.43	0.41	0.41
	Std. Dev.	[°]	0.24	0.19	0.19

Table 3. Calibration Performance Comparative Metrics, Measured B-Field vs Reference B-Field Vectors, 2010

2010			**Former WLSM**	**New MLE, Optimal Alignment**	**New MLE, Mean Alignment**
X axis	**Avg.**	**[mG]**	0.22	0.12	0.12
	Std. Dev.	**[mG]**	1.67	1.46	1.46
	Avg.+3σ	**[mG]**	5.23	4.57	4.57
Y Axis	**Avg.**	**[mG]**	0.02	-0.13	-0.13
	Std. Dev.	**[mG]**	1.56	1.36	1.36
	Avg.+3σ	**[mG]**	4.87	4.25	4.24
Z Axis	**Avg.**	**[mG]**	0.14	0.28	0.28
	Std. Dev.	**[mG]**	1.70	1.55	1.55
	Avg.+3σ	**[mG]**	5.24	4.93	4.94
RSS	**Avg.+3σ**	**[mG]**	8.89	7.98	7.98
Final Angle	**Avg.**	[°]	0.47	0.40	0.40
	Std. Dev.	[°]	0.16	0.19	0.19

Table 4. Calibration Performance Comparative Metrics, Measured B-Field vs Reference B-Field Vectors, 2011

2011			Former WLSM	New MLE, Optimal Alignment	New MLE, Mean Alignment
X axis	**Avg.**	**[mG]**	0.22	-0.08	-0.08
	Std. Dev.	**[mG]**	1.76	1.31	1.31
	Avg.+3σ	**[mG]**	5.50	4.14	4.14
Y Axis	**Avg.**	**[mG]**	0.00	-0.17	-0.17
	Std. Dev.	**[mG]**	1.53	1.23	1.24
	Avg.+3σ	**[mG]**	4.75	3.92	3.94
Z Axis	**Avg.**	**[mG]**	0.11	0.21	0.21
	Std. Dev.	**[mG]**	1.84	1.38	1.38
	Avg.+3σ	**[mG]**	5.64	4.35	4.36
RSS	**Avg.+3σ**	**[mG]**	9.23	7.20	7.22
Final Angle	**Avg.**	[°]	0.43	0.36	0.36
	Std. Dev.	[°]	0.25	0.18	0.18

Table 5. Calibration Performance Comparative Metrics, Measured B-Field vs Reference B-Field Vectors, 2012

2012			Former WLSM	New MLE, Optimal Alignment	New MLE, Mean Alignment
X axis	**Avg.**	**[mG]**	0.26	0.02	0.02
	Std. Dev.	**[mG]**	2.68	1.79	1.78
	Avg.+3σ	**[mG]**	8.30	5.53	5.53
Y Axis	**Avg.**	**[mG]**	0.03	-0.15	-0.15
	Std. Dev.	**[mG]**	2.41	1.49	1.49
	Avg.+3σ	**[mG]**	7.48	4.66	4.67
Z Axis	**Avg.**	**[mG]**	0.26	0.19	0.19
	Std. Dev.	**[mG]**	2.76	1.72	1.73
	Avg.+3σ	**[mG]**	8.55	5.35	5.39
RSS	**Avg.+3σ**	**[mG]**	14.19	9.08	9.12
Final Angle	**Avg.**	[°]	0.76	0.45	0.45
	Std. Dev.	[°]	0.31	0.28	0.28

Table 6. Calibration Performance Comparative Metrics, Measured B-Field vs Reference B-Field Vectors, 2013

2013			Former WLSM	New MLE, Optimal Alignment	New MLE, Mean Alignment
X axis	**Avg.**	**[mG]**	0.25	-0.21	-0.21
	Std. Dev.	**[mG]**	1.88	1.16	1.17
	Avg.+3σ	**[mG]**	5.89	3.76	3.79
Y Axis	**Avg.**	**[mG]**	-0.03	-0.20	-0.18
	Std. Dev.	**[mG]**	1.66	1.19	1.19
	Avg.+3σ	**[mG]**	5.11	3.78	3.76
Z Axis	**Avg.**	**[mG]**	0.10	0.18	0.16
	Std. Dev.	**[mG]**	2.05	1.26	1.26
	Avg.+3σ	**[mG]**	6.29	3.96	3.95
RSS	**Avg.+3σ**	**[mG]**	10.05	6.70	6.70
Final Angle	**Avg.**	[°]	0.48	0.34	0.34
	Std. Dev.	[°]	0.26	0.15	0.15

Table 7. Calibration Performance Comparative Metrics, Measured B-Field vs Reference B-Field Vectors, 2014

2014			Former WLSM	New MLE, Optimal Alignment	New MLE, Mean Alignment
X axis	**Avg.**	**[mG]**	0.28	-0.27	-0.27
	Std. Dev.	**[mG]**	1.15	1.11	1.01
	Avg.+3σ	**[mG]**	3.74	3.69	3.59
Y Axis	**Avg.**	**[mG]**	-0.03	-0.18	-0.20
	Std. Dev.	**[mG]**	1.28	1.33	1.34
	Avg.+3σ	**[mG]**	3.99	4.19	4.23
Z Axis	**Avg.**	**[mG]**	0.19	0.09	0.10
	Std. Dev.	**[mG]**	1.38	1.38	1.38
	Avg.+3σ	**[mG]**	4.35	4.32	4.30
RSS	**Avg.+3σ**	**[mG]**	7.16	7.20	7.18
Final Angle	**Avg.**	[°]	0.35	0.36	0.36
	Std. Dev.	[°]	0.15	0.15	0.16

Table 2 through Table 7 present comparative metrics for the performance of the new algorithm, both with optimal alignment and mean alignment, along with that of the former WLSM methodology as a basis (which was re-run anew for comparison integrity; released reports values were not retrieved exactly due to small dataset variations). It may be observed that since for the attitude-independent scheme only the B-field magnitude is used in balancing the parameters, it is prone to elect a different strategy from the previous methodology. While the latter appears to have focused on improving the Y-axis, the new algorithm chiefly improves the X-axis. Such differences can be reviewed in light of the ADCS particulars, if as is the case for SCISAT, precision along different axes may or may not be equally desirable.

As a side note and a caveat, an account of the impact of convergence thresholds criteria can further be presented. In the early phases of testing, the MLE algorithm computation was left running until relatively stringent stability criteria were met (3 subsequent iterations below 0.00001 evolution on any T-Matrix element and 0.001 on any b-vector element). The results were featuring quite significant scatter, needing frequent outliers exclusion, and it became obvious that the solution set could jump in values by significant magnitudes after having converged rather precisely, to converge again – with comparatively nonsensical precision – at the new values set, and walk indefinitely in such manner in a neighbourhood that appeared arguably too sizeable for practical application. While no comprehensive nor conclusive analysis or characterization of such numerical difficulties was performed, Fig. 5 demonstrates the dramatic change in behaviour that occurred after relaxing the convergence criteria (stopping after the *first* iteration meeting the same thresholds), whereafter literally every run of all datasets did converge in exactly the same amount of steps (4) and with considerably increased consistency. Moreover, this testimony of reliability in the results was obtained for a starting state vector not as close as it could be from the endpoint. Testing at closer initial estimates also featured, to a lesser extent, the presence of outliers, less systematic convergence, and a worse scatter from the mean alignment.

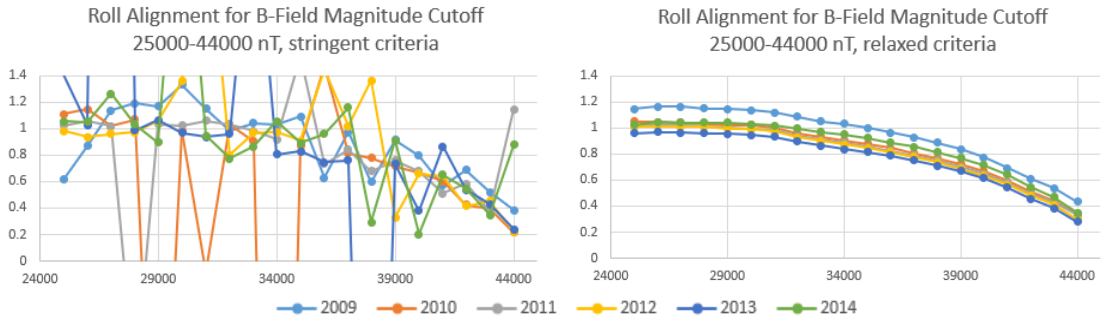

Fig. 5. Roll Optimal Alignment Angle [°] vs Dataset Magnitude Cutoff, for two convergence thresholds criteria sets, same scale

3.3 Flight Implementation

Using the established mean alignment, the computation was carried out on the most recent 2023 and 2024 datasets. As apparent from Fig. 6, the resulting prescribed calibration parameters appeared to have known the most significant evolution for the on-diagonal elements of the T-matrix, which incidentally would be little influenced by any small-angle drift in pure rotation. This could signify a genuine need of re-calibration, a shift in strategy in balancing the axis-wise errors, or evidently a mixture of both. Since the new points look consistent with the trends of the 2009-2014 results of the new algorithm, which visibly possesses different slopes than those of the results previously achieved, it is conjectured that the second explanation is the most determinant. The fact that in Table 2 through Table 7, the new paradigm is seen to frequently beat the former one in most metrics may advocate the legitimacy of the change.

However, the cohesive character of the solutions found by the algorithm is assumed to be paramount due to the outstanding mean alignment philosophy restriction. Any break in trends would be regarded as suspicious, since it could be expected that latching onto a different strategy in balancing the axis-wise errors could involve a different mean alignment, possibly leading to an incorrect calibration if applied without validity.

As expected, it is observable in Fig. 6 and Fig. 7 that only the off-diagonal elements of the T-matrix exhibit a visible departure of the mean alignment calibration from the optimal alignment calibration. Note that the figures depict the rotated (aligned) T-Matrix and compound bias vector, meaning the P-Matrix and d-vector of equation (21).

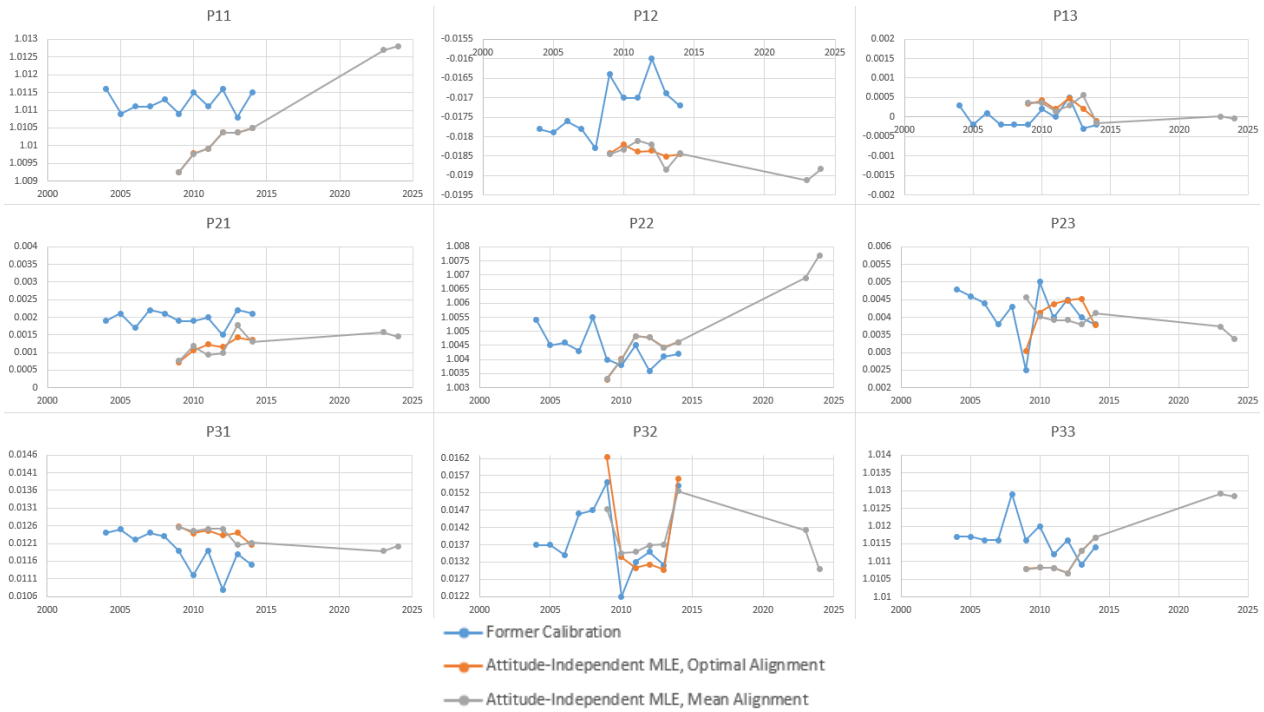

Fig. 6. Rotated T-Matrix (P-Matrix) Parameters Evolution (by Matrix Element)

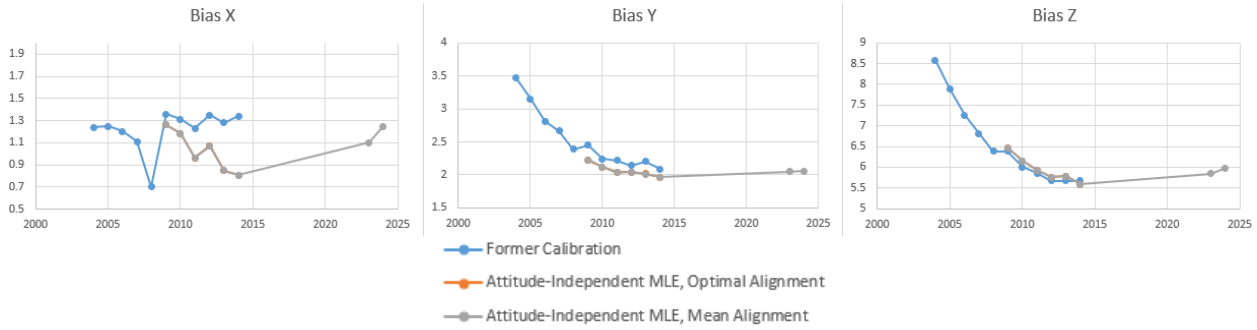

Fig. 7. Biases Vector (d-Vector) Parameters Evolution (by Element), mG

Preliminary analysis on theoretical attitude errors re-composition accounting for the new adjustments indicated an improvement in mean Roll attitude errors was likely and the expected maximum attitude angle deviation generated by the update from the current settings (at the time) for a typical day was small – estimated at 0.005 rad for Doy 2025-049).

On the basis of the above, the newly determined set of calibration parameters from the 2024 dataset was implemented in flight for testing on Feb 27th 2025 (2025-056). Data is currently being collected following this implementation, with the perceived attitude errors deviations serving as the main (indirect) means of assessing performance. Table 8 presents the early results of this testing phase for 2025, where slightly less than half a beta cycle was used in extracting comparatives to the years 2024 and 2014 (the last year of the former calibration process), for the same beta angles interval.

Table 8. Attitude errors comparatives for the corresponding first half beta cycle before and after implementation

	|avg|+3σ [rad]		
	X	**Y**	**Z**
2014	0.009867	0.00692	0.012245
2024	0.009631	0.012076	0.013167
2025	0.005731	0.011003	0.01325

These early results tend to show that the re-calibration indeed led to an improvement in Roll attitude errors, and a less substantial improvement in Pitch, despite a still smaller degradation in Yaw. As expected, the overall performance does not seem to be as optimal as for the year 2014, on account of the probable small residual rotation unknown error caused by the use of a mean alignment.

It may be noted that the perspective of complementing the algorithm implementation by means of the Fine Sun Sensor (FSS) telemetry could be contemplated. In this case, a small SO(3, $\mathbb{R}$) corrective could be solved for timespans of FSS availability; for Pitch and Yaw, it is expected that this could be achieved without deterring the Spacecraft from its nominal attitude, and using the existing telemetry for offline processing, thanks to small angles simplifications. Such a fine-tuning on the alignment component simplifies considerably the otherwise more complex matter of devising an entire calibration scheme based solely on the FSS readings to produce the necessary attitude determination, provided that this sensor also solves for a single vector at any given time. It is not yet known with certainty, however, to what extent the alignment can be further tuned, conceding that the optimal parameters are time-varying and that the aiding sensor's availability is limited to half the orbit in the timeframe of interest. Further analyses would be needed in this respect, as for the possibilities to better harness the implications of the initial state vector selection.

4. Conclusions

The ongoing efforts to re-instantiate magnetometer calibration and improve attitude determination are part of the prophylactic activities aimed at ensuring continued accuracy and reliability of the data collected by SCISAT, after over twenty years of operation.

Despite some numerical and conceptual shortcomings, notably with respect to the final alignment issue of the results found in the sensor frame, the studied Attitude-Independent algorithm [1, 2], extended to the case of varying reference magnetic field, was demonstrated to be capable of adequate (near-optimal) performance close to the timeframe of supplementary equipment availability – at least in the case of SCISAT which circumstances and a relatively loose pointing budget seemingly made a good candidate – and the trend has so far continued to hold after a decade of possible drift, as observed from the early results of the recent flight test implementation. Albeit not as optimal as the former calibration scheme, as was expected due to the current alignment possibilities, it already appears capable of bringing back down to some extent the perceived attitude errors that had undergone a slight degradation since the magnetometer was last calibrated. It is therefore hoped to allow for an improvement of the attitude disturbances experienced in the recent years.

It is not yet known with certainty whether the new calibration will continue to consistently achieve convergence on affiliated solution sets or whether the mean alignment, as implemented, is to undergo some continued degradation, but the current results suggest that the magnetometer calibration could be re-instantiated back into yearly routine activities, the cumulated inaccuracy of the method being so far shown smaller than the effect of parameter drift.

References

[1] J. F. Vasconcelos, G. Elkaim, C. Silvestre, P. Oliveira, and B. Cardeira, Geometric approach to strapdown magnetometer calibration in sensor frame, IEEE Trans. Aerosp. Electron. Syst., vol. 47, no. 2, pp. 1293–1306, Apr. 2011

[2] Y. Wu, W. Shi, On calibration of three-axis magnetometer, IEEE Sensors J., vol. 15, no. 11, pp. 6424–6431, Nov. 2015.

[3] C. C. Foster, G. H. Elkaim, Extension of a two-step Calibration Methodology to include Nonorthogonal Sensor Axes, IEEE Transactions on Aerospace and Electronic Systems, 44, 3 (July 2008), 1070-1078

[4] J. C. Springmann, J. W. Cutler, Attitude-Independent Magnetometer Calibration with Time-Varying Bias, Journal of Guidance, Control, and Dynamics, vol. 35, no. 4, Jul.-Aug. 2012

[5] A. E. Bryson, Yu-Chi Ho, Applied Optimal Control, Revised Printing, Hemisphere Publishing, Washington D.C., 1975, pp.349-359

[6] Magellan Aerospace, TN.ADCS.0018/A, SCISAT ACE Mission ADCS On Orbit Calibration Algorithms

[7] R. Alonso, M. D. Shuster, TWOSTEP: A Fast Algorithm for Attitude-Independent Magnetometer-Bias Determination, The Journal of Astronautical Sciences, vol. 50, no. 4, Oct.-Dec. 2002, pp. 433-451

[8] R. Alonso, M. D. Shuster, Complete Linear Attitude-Independent Magnetometer Calibration, The Journal of Astronautical Sciences, vol. 50, no. 4, Oct.-Dec. 2002, pp. 477-490

[9] Magellan Aerospace, ER-100459/A, SCISAT-1 / ACE Mission ADCS Detailed Pointing Budget Analysis, Jan. 2002

[10] F. J. Lowes, IGRF Health Warning, Errors, and Limitations, 22 May 2022, https://www.ncei.noaa.gov/products/international-geomagnetic-reference-field/health-warning, (accessed 30.03.25).